Earthq Eng & Eng Vib (2014) 13: 47-57 **DOI**: 10.1007/s11803-014-0211-7

Experimental study on the seismic behavior of high strength concrete filled double-tube columns

Qian Jiaru†, Li Ningbo‡, Ji Xiaodong§, Zhao Zuozhou§

Key Laboratory of Civil Engineering Safety and Durability of China Education Ministry, Department of Civil Engineering, Tsinghua University, Beijing 100084, China

Abstract: To study the seismic behavior of high strength concrete filled double-tube (CFDT) columns, each consisting of an external square steel tube and an internal circular steel tube, quasi-static tests on eight CFDT column specimens were conducted. The test variables included the width-to-thickness ratio (β_1) and the area ratio (β_2) of the square steel tube, the wall thickness of the circular steel tube, and the axial force (or the axial force ratio) applied to the CFDT columns. The test results indicate that for CFDT columns with a square steel tube with β_1 of 50.1 and 24.5, local buckling of the specimen was found at a drift ratio of 1/150 and 1/50, respectively. The lateral force-displacement hysteretic loops of all specimens were plump and stable. Reducing the width-to-thickness ratio of the square steel tube, increasing its area ratio, or increasing the wall thickness of the internal circular steel tube, led to an increased flexural strength and deformation capacity of the specimens. Increasing the design value of the axial force ratio from 0.8 to 1.0 may increase the flexural strength of the specimens, while it may also decrease the ultimate deformation capacity of the specimen with β_1 of 50.1.

Keywords: high strength concrete filled double-tube (CFDT) column; seismic behavior; area ratio of the square steel tube; width-to-thickness ratio of the square steel tube; axial force ratio; quasi-static test

1 Introduction

Concrete filled steel tube (CFT) columns have been widely used in the construction of underground structures, multi-story buildings, high-rise buildings, large span structures, bridges, and other supporting structures. CFT columns offer significant advantages over either reinforced concrete columns or steel columns. The steel tubes provide formwork and reinforcements to the concrete, prevent excessive crushing and spalling of concrete, and minimize the cost of the concrete placement. Concrete placed inside the CFT columns provides compressive strength and stiffness and postpones local buckling of the steel tube. For CFT columns with a circular section, the confinement effect of the steel tube not only provides the column with high load carrying-capacity and large ductility, but also allows it to utilize the high strength concrete, resulting in smaller size columns. The CFT columns with a circular section were invented in 1897 and used in some low-rise buildings and bridges in the early 20th century. Extensive investigations on their mechanical behavior were conducted in the 1950s and 1960s (Garder and Jacobson, 1967; Knowles and Park, 1969). Since the 1980s, extensive experimental and theoretical studies on the seismic performance of CFT columns and on the mechanical behavior of high strength concrete filled steel tube columns with square and circular sections have been carried out (Rangan and Joyce,1992; Varmar *et al*., 2004; Eiichi *et al.*, 2004; Cai and Jiao, 1984; Zhong and Wang, 1980; Zhang and Zuo, 1985). In latter half of the 1980s, the technology of pumping concrete and the development of high strength concrete made the utilization of CFT columns in high-rise buildings possible. Many high-rise buildings in the U.S, Japan, Austria and China (Randall and Foot, 1989; Webb and Peyton,1990; Sugiki *et al.*,1998; and Cai, 1999) adopted CFT columns as one of the main structural elements for earthquake resistance. Among these high-rise buildings, the tallest is the SEG Plaza, with 72-stories, 293 m high above the ground, and located in Shenzhen, China (Wu and Hua, 2002).

Almost all of the research and applications of CFT columns are concrete filled single-tube columns. Sometimes, concrete filled double-tube (CFDT) columns are needed. It was reported by Roik and Bergmann (1985) that for the Wuppertal city municipal building, the vertical load carried by the column was 8000 kN, while the diameter of the column was limited to no larger than 600 mm. At the same time, the columns

Correspondence to: Qian Jiaru, Department of Civil Engineering, Tsinghua University, Beijing 100084, China
Tel: +86-10-62788620; Fax: +86-10-62788620
E-mail: qianjr@tsinghua.edu.cn
†Professor; ‡Assistant Researcher; §Associate Professor

Supported by: the National Natural Science Foundation of China under Grants Nos. 51261120377 and 51008173
Received April 7, 2013; **Accepted** September 28, 2013

were required to have sufficient fire resistance. To meet these requirements, CFDT columns with both external and internal circular steel tubes were used. CFDT columns offer all of the advantages of CFT columns, and in addition, the internal CFT provides a second defense line for resisting fire, impact, blast and earthquakes. The robustness of the collapse resistance of CFDT columns is increased by the internal CFT. Until now, only a few studies on the mechanical behavior and seismic performance of CFDT columns have been reported. Liew and Xiong (2012) carried out an experimental investigation on 27 axially loaded column specimens with circular sections, including five hollow steel tubes for comparison, 14 concrete filled single-tube columns to study the application of ultra-high strength concrete in columns, and 8 concrete filled double-tube columns with internal circular steel tubes for potential application in multi-story and high-rise buildings. The mechanical behavior of CFDT columns with an external square steel tube and an internal circular steel tube (Fig.1) has been recently studied in China. Lü and Zhao (2001) performed a numerical analysis on the compression-bending behavior of CFDT columns and concluded that the inner circular steel tube enhanced the eccentric compressive strength capacity of the column. Pei (2005) carried out concentric and eccentric compressive loading tests on six CFDT column specimens and concluded that the tubes had a confinement effect and the column had composite action. Based on the test results of Pei (2005), and applying the unified theory, Zhang *et al.* (2009) established an axial compressive strength formula for CFDT columns. Qian *et al.* (2012) carried out axial compressive loading tests on 23 high strength CFDT short columns and proposed the axial compressive strength formula for CFDT columns.

In this study, quasi-static tests on eight high strength concrete filled double-tube columns with an external square steel tube and an internal circular steel tube (Fig.1) are introduced. The test columns are called CFDT columns, and the words 'high strength' and 'with external square steel tube and internal circular steel tube' do not appear in the abbreviation. The objective of the tests is to examine the seismic behavior focusing on the influence of parameters on the seismic behavior of CFDT columns.

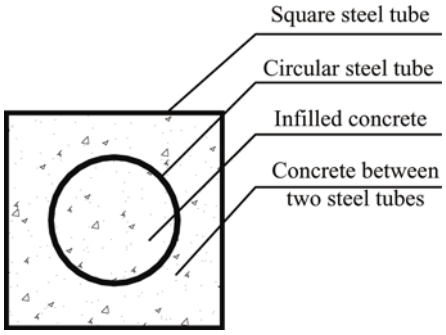

Fig. 1 Cross-section of CFDT column with external square steel tube and internal circular steel tube

2 Experimental program

2.1 Test specimens

2.1.1 Specimens design

Eight CFDT column specimens, labelled C1-0.8 through C8-1.0, were tested. The specimens were designed to represent the lower story CFDT columns in high-rise buildings, and were fabricated at approximately 1/4 scale to accommodate the capacity of the loading facility. The overall geometries of the CFDT column specimens are showed in Fig. 2a. Each specimen had a base footing and a CFDT column. The former has a cross-section of 600 mm × 650 mm (width × height). The CFDT column had a square steel tube of 300 mm by 300 mm, a circular steel tube with diameter of 219 mm, and a height of 1410 mm. The square steel tube and the circle steel tube were extended into the base footing to achieve a full anchorage. The anchorage depth was 600 mm, two times the cross-section height of the square steel tube. In addition, a steel cover plate with triangle stiffeners was welded at the steel tube bottom, and two rows of deformed re-bars were welded along the square steel tube perimeter and the circular steel tube perimeter as rib bars, which contributed to a secure anchorage.

2.1.2 Material strength

Concrete with the same strength was used to fill the circular steel tube and the space in between two tubes. The concrete strength for each specimen is listed in Table 1. For each specimen, three concrete cubes of 150 mm size were tested to obtain the measured mean value of

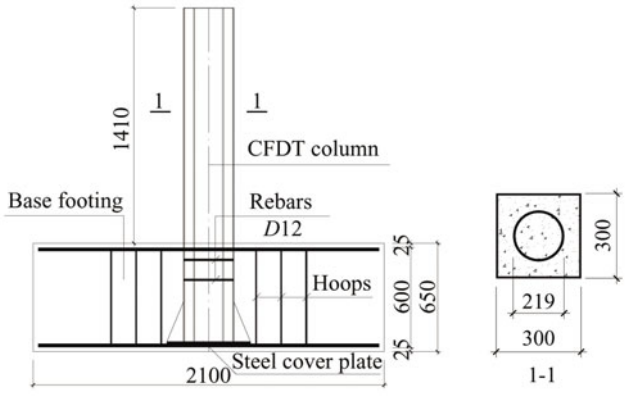

(a) Elevation view of specimens

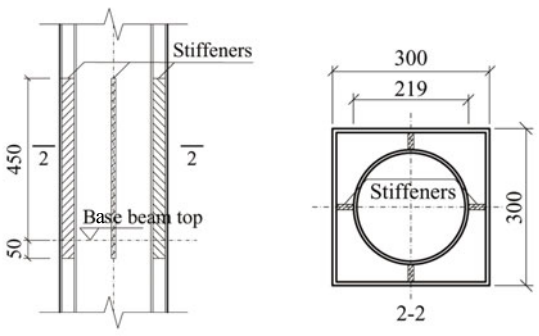

(b) Arrangement of inner stiffeners for specimens C5-0.8 to C8-1.0

Fig. 2 Configuration and details of specimens

cubic compressive strength $f_{cu,m}$. The square deviation δ of 24 cubes was 0.039. The standard cubic compressive strength $f_{cu,k}$, which represents the concrete strength grade, was calculated by using the expression $f_{cu,k} = f_{cu,m}(1\text{-}1.645\delta)$, and the measured axial compressive strength $f_{c,m}$ was calculated by $f_{c,m} = (0.66 + 0.002 f_{cu,k}) f_{cu,m}$ (Ye, 2012). Based on $f_{cu,k}$, the design value of axial compressive strength $f_{c,d}$ was obtained from the Chinese Code for Design of Concrete Structures (2010).

All the square and circular steel tubes were fabricated from Q235 steel. The design strength of Q235 steel was taken as 210 MPa. The measured material strength of the steel tubes are listed in Table 2, where t denotes the wall thickness of the tube or the thickness of the inner stiffener, $f_{s,m}$ and $f_{a,m}$ denote the measured material yield strength of the square steel tube and the circular steel tube, respectively, and $f_{u,m}$ is the measured material ultimate strength of the steel tubes. The yield strain ε_y of the steel material is also listed in Table 2, which was calculated by the following formula, $\varepsilon_y = f_{s,m}/E$ or $f_{a,m}/E$, here E is the modulus of elasticity of steel, E=2.0×10^5 MPa.

Table 1 Concrete strength MPa

Specimen No.	$f_{cu,m}$	$f_{cu,k}$	$f_{c,m}$	$f_{c,d}$
C1-0.8	83.6	78.2	68.3	35.1
C2-1.0	77.6	72.6	62.5	32.9
C3-0.8	86.5	80.9	71.1	36.2
C4-0.8	79.2	74.1	64.0	33.5
C5-0.8	75.2	70.4	60.2	31.9
C6-1.0	75.8	70.9	60.7	32.2
C7-0.8	75.8	70.9	60.7	32.2
C8-1.0	78.4	73.3	63.2	33.2

Table 2 Measured steel material strength and yield strain of steel material

Member type	t (mm)	$f_{s,m}$ or $f_{a,m}$ (MPa)	$f_{u,m}$ (MPa)	ε_y (10^{-6})
Square steel tube	5.76	305.5	429.4	1528
	7.65	352.6	484.8	1763
Circular steel tube	5.62	367.7	473.4	1838
	6.02	329.5	438.4	1647
	9.57	325.2	500.6	1626
Inner stiffener	5.69	299.7	462.3	1499

2.2 Test variables

Table 3 shows the main parameters of the CFDT columns. Four test variables were considered: wall width-to-thickness ratio (β_1) and area ratio (β_2) of the square steel tube, wall thickness of the circular steel tube, and axial force (or axial force ratio) applied to the columns. Details of variables are described as follows.

In Table 3: (1) the numerals 0.8 and 1.0 in the Specimen No. column denote the expected design axial force ratios of the test columns; (2) t_1 and t_2 denote the wall thicknesses of the square and circular steel tubes, respectively; (3) β_1 denotes the width-to-thickness ratio of the square steel tube, $\beta_1=b_1/t_1$, where b_1 denotes the wall net width of the square steel tube; (4) β_2 denotes the area ratio of the square steel tube, $\beta_2=A_s/A$, A_s and A denote the cross-section area of the square steel tube and the CFDT column; (5) θ_c denotes the confinement index of the concrete filled circular steel tube, $\theta_c=f_aA_a/(f_cA_{cc})$, where f_a and A_a represent the material yield strength and the cross-section area of the circular steel tube, respectively, f_c and A_{cc} represent the axial compressive strength and the cross-section area of the concrete filled in circular steel tube, respectively; (6) N and n are the axial compressive force and the axial force ratio applied to the column, respectively; and (7) subscripts d and t represent the design value and the test value, respectively. In calculation of $\theta_{c,d}$ and n_d, the design value of f_a and f_c are used, while in calculation of $\theta_{c,t}$ and n_t, the measured value of f_a and f_c are used.

2.2.1 Width-to-thickness ratio of the square steel tube

As shown in Table 1, the specimens had three different values of width-to-thickness ratio β_1 for the square steel tube. Specimens C1-0.8 through C3-0.8 had a β_1 value of 50.1. Specimen C4-0.8 had a smaller β_1 value of 37.2 because it used a thicker tube. Although specimens C5-0.8 through C8-1.0 had the same geometry as specimens C1-0.8 through C3-0.8, the value of β_1 was reduced to approximately half due to the additional vertical stiffeners inside of the square steel tube. The purpose of addition of the inner stiffeners was to postpone local buckling of the external square steel tube. The arrangement of the inner stiffeners is shown in Fig. 2(b). The thickness of inner stiffeners was 5.69 mm and the in-height length was 1.5 times the column section width, i.e., 1.5 times the expected column plastic

Table 3 Main parameters of specimens

Specimen No.*	Square tube			Circular tube			Axial force N (kN)	Axial force ratio	
	t_1 (mm)	β_1	β_2 (%)	t_2 (mm)	$\theta_{c,d}$	$\theta_{c,t}$		n_d	n_t
C1-0.8	5.76	50.1	7.68	5.62	0.68	0.60	3520	0.78	0.37
C2-1.0				5.62	0.73	0.65	4180	0.95	0.46
C3-0.8				9.57	1.19	0.92	4035	0.77	0.38
C4-0.8	7.65	37.2	10.2	5.62	0.71	0.64	3768	0.74	0.35
C5-0.8	5.76	24.5	7.68	6.02	0.81	0.65	3412	0.78	0.39
C6-1.0					0.80	0.65	4065	0.92	0.46
C7-0.8					0.80	0.65	3423	0.78	0.39
C8-1.0					0.78	0.62	4142	0.93	0.46

hinge length. For specimens C5-0.8 and C6-1.0, the inner stiffeners were welded to the square steel tube only, whereas for specimens C7-0.8 and C8-1.0, the inner stiffeners were welded to the square steel tube and to the circular steel tube.

2.2.2 Area ratio of the square steel tube

The area ratio of the square steel tube is defined as the cross-section area ratio of the square steel tube to the CFDT column. The area ratio was 10.2% for specimen C4-0.8 and 7.68% for the other specimens.

2.2.3 Thickness of the circular steel tube

All circular steel tubes of the specimens had an identical diameter. The circular tube of specimen C3-0.8 had the largest thickness among all the specimens.

2.2.4 Axial force ratio

The axial force ratio of the CFDT column specimens is defined as follows:

$$n_d=1.2N/(f_{s,d}A_s+f_{c,d}A_{co}+0.9f_{c,d}A_{cc}(1+1.8\theta_{c,d})) \quad (1a)$$

$$n_t=N/(f_{s,m}A_s+f_{c,m}A_{co}+0.9f_{c,m}A_{cc}(1+1.8\theta_{c,t})) \quad (1b)$$

where $f_{s,d}$ denotes the design strength of the square steel tube material; A_{co} denotes the cross-section area of the concrete filled in between tubes. When the vertical load combines with the lateral seismic action, the load factor (i.e., the ratio of design value to standard value of the load) is 1.2 and 1.3, respectively, according to the Chinese technical specification for concrete structures of tall building (2010). Thus, in Eq.1a, to calculate n_d of the column specimens, the axial compressive force factor was taken as approximately 1.2. Also in Eq.(1a), $0.9f_{c,d}A_{cc}(1+1.8\theta_{c,d})$ is the design value of the axial compressive strength of the concrete filled circular steel tube column according to the Chinese technical specification for concrete structures of tall building (2010). To calculate n_t of the column specimens, the axial compressive force factor was taken as 1.0 as shown in Eq. (1b).

2.3 Test setup and loading program

2.3.1 Test setup

The specimens were placed in a loading frame, and the test column was loaded as a cantilever, as shown in Fig. 3. The base footing of the specimen was securely clamped to the reaction floor. The column was clamped at its top to a vertical hydraulic jack and a horizontal hydraulic actuator.

The lateral force was applied by a hydraulic actuator. The center axis of the actuator was 1200 mm and 1250 mm height from the column bottom for specimens C1-0.8 through C4-0.8 and for specimens C5-0.8 through C8-1.0, respectively. The column had a shear-to-span ratio of 4.0 or 4.17, ensuring a flexure-dominated deformation mode.

2.3.2 Loading program

A vertical load was applied to the top of the CFDT column at the beginning of the test and was maintained constant throughout the duration of the test. Then, cyclic lateral forces were applied quasi-statically by the horizontal actuator.

Figure 4 shows the lateral loading history for the test. The lateral loading was controlled by the CFDT column top drift ratio θ_d. The drift ratio θ_d is defined as $\theta_d=\Delta/H$, where Δ is the column top lateral displacement, H is its measurement height from the column bottom, i.e., 1200 mm and 1250 mm for specimens C1-0.8–C4-0.8 and specimens C5-0.8–C8-1.0, respectively. At each level of the drift ratio θ_d of 1/1000, 1/500 and 1/300, one cycle was performed. At each level of the drift ratio θ_d of 1/200, 1/150, 1/100, /1/75, 1/50 and 1/33, three cycles were performed. At the level of drift ratio θ_d of 1/25, two cycles or one cycle was performed.

2.4 Instrumentation

Instruments were used to measure loads, displacements and strains for specimens. Load cells were used to measure the vertical load and the lateral forces applied to the specimens. Five linear variable differential transformers (LVDTs) were mounted to measure the lateral displacements at 300 mm intervals over the column height. A LVDT was mounted horizontally on the base footing to monitor any horizontal slip of the base footing along the reaction floor. No slippage was observed during the test. Twelve LVDTs were applied to

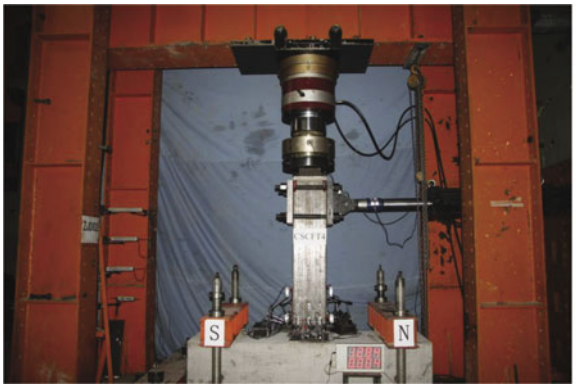

(a) Photograph of experiment site

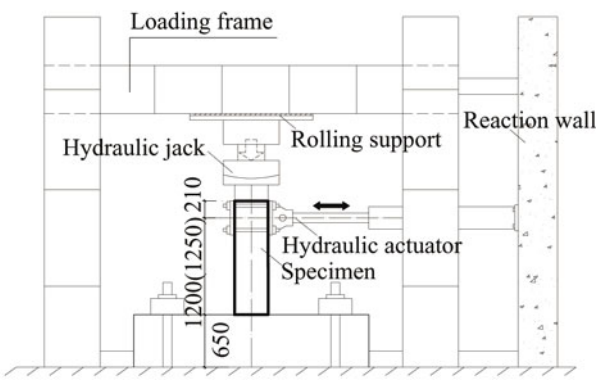

(b) Test set-up

Fig. 3 Photograph of experiment site and test set-up

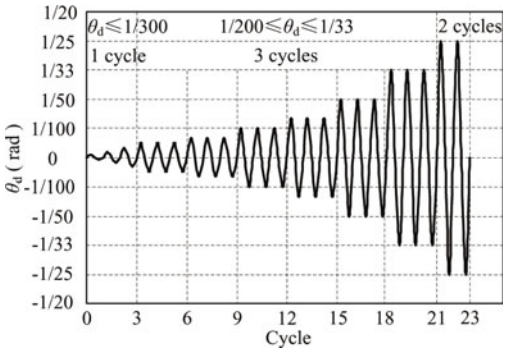

Fig. 4 Target drift ratio history

measure the vertical deformation of the column over a height of 300 mm from the column bottom, from which the averaged strains could be estimated. The strains of the square steel tube and the circular steel tube were measured by strain gauges. All the strain gauges were located approximately 30 mm above the column bottom. The measurements were recorded by a computer data acquisition system.

3 Experimental results

3.1 Damage process and failure mode

Specimens C1-0.8 through C4-0.8 showed similar damage development and failure mode. Note that the square steel tube of specimens C1-0.8 through C3-0.8 had a β_1 value of 50.1, specimen C4-0.8 had a relatively lower β_1 value of 37.2. At the 1/150 drift ratio, local outward buckling was observed at the compressive flange of the square steel tube. Local buckling deformation at the flange could recover when the lateral force reversed. At the 1/100 drift ratio, local outward buckling of the compressive flange of the square steel tube was obvious within a height of 75 mm-125 mm from the column bottom. When θ_d was about 1/75, residual buckling deformation of the flange was found, and local buckling of the web occurred. When θ_d was about 1/50, outward local buckling at the corner of the square steel tube was observed.

After the tests, the square steel tube and concrete in between tubes at the lower part of columns were removed, and the failure mode of concrete in between tubes and of the circular tube was observed. Figure 5 shows photographs of specimen C3-0.8 after tests. The failure mode of the specimens C1-0.8 through C4-0.8 is summarized as follows: significant local buckling of the square steel tube, compressive crushing of the concrete filled in between tubes within a height of about 150 mm from the column bottom, and slight buckling of the circular steel tube.

Specimens C5-0.8 through C8-1.0 had a β_1 value of 24.5. At the 1/100 drift ratio, local buckling of the square steel tube was not found. Until the drift ratio reached 1/50, outward buckling of the square steel tube was observed. Figure 6 shows photographs of specimens C5-0.8 and C7-0.8 after tests. For specimens C5-0.8 through C8-1.0, residual buckling deformation of the square steel tube was smaller than that of specimens C1-0.8 through C4-0.8.

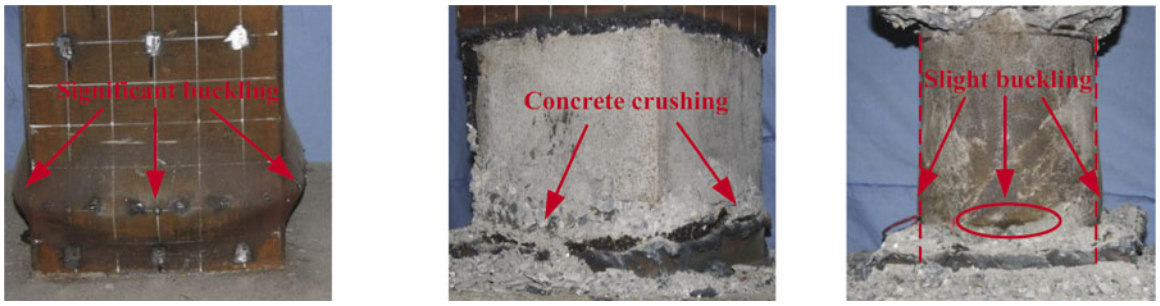

(a) Square steel tube (b) Concrete between steel tubes (c) Circular steel tube

Fig. 5 Photographs of specimen C3-0.8 after tests

(a) C5-0.8 (b) C7-0.8

Fig. 6 Photographs of specimen C5-0.8 and C7-0.8 after tests

3.2 Lateral force-displacement relationship

Figure 7 shows the column bottom moment versus column top drift ratio (M-θ_d) hysteresis loops for all eight specimens. Considering the second order effects of axial force applied on the column top, the column bottom moment is calculated by the following relationship:

$$M=PH_1+N\Delta \tag{2}$$

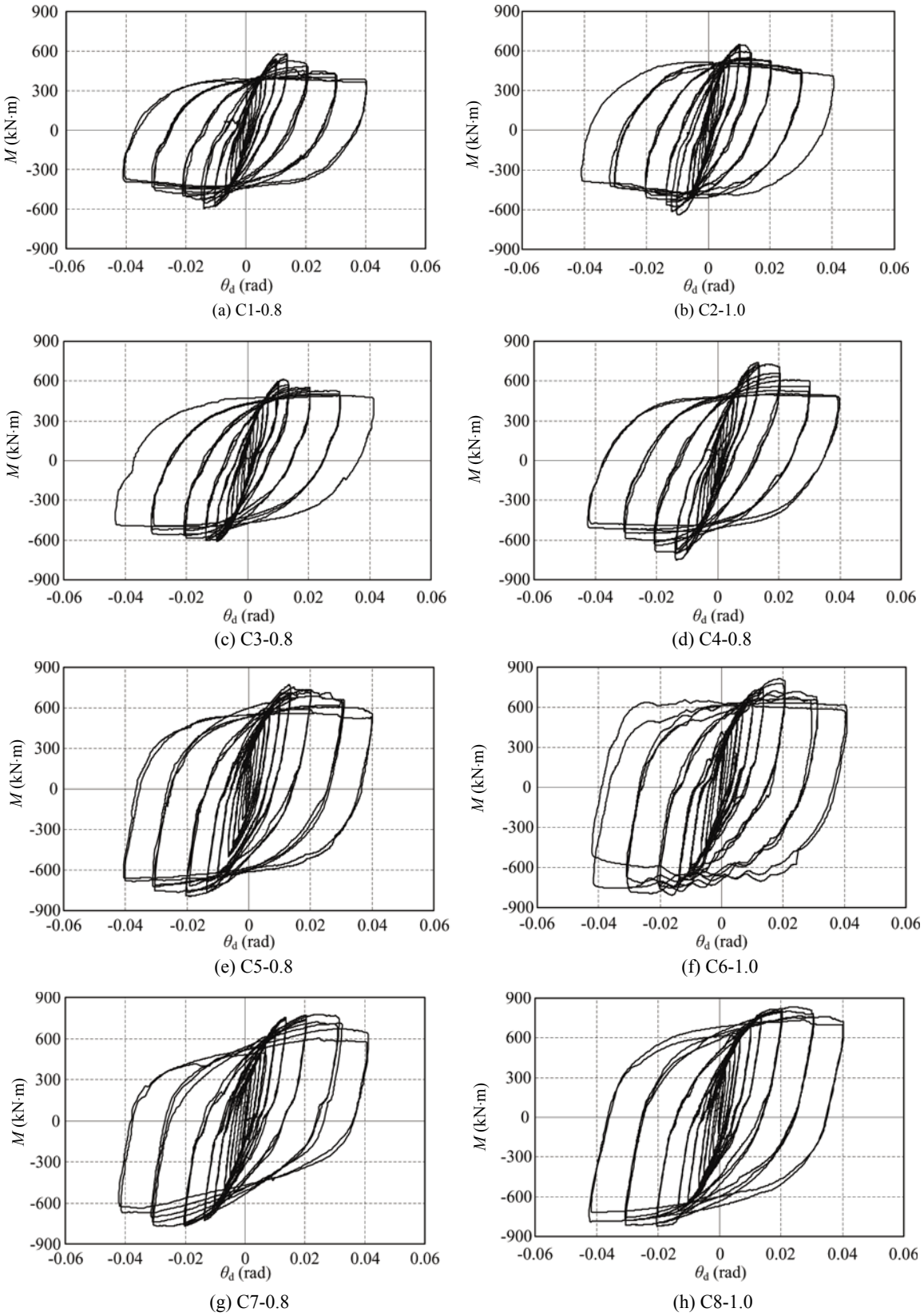

(a) C1-0.8 (b) C2-1.0

(c) C3-0.8 (d) C4-0.8

(e) C5-0.8 (f) C6-1.0

(g) C7-0.8 (h) C8-1.0

Fig. 7 Moment-drift ratio (M-θ_d) hysteretic loops of specimens

in which M denotes the column bottom moment, P denotes the measured lateral force applied at the top of the column, H_1 denotes the lateral force height measured from the column bottom, N is the axial compressive force applied on the column top as listed in Table 3, and Δ is the measured column top lateral displacement. The loops of all specimens were plump and stable, showing the inherent large energy dissipation capacity of CFDT columns. When loading and unloading within a small drift ratio (less than 1/500), the hysteresis curves cycled almost linearly without residual deformation. When θ_d was larger than 1/300, residual drift ratio was observed during unloading.

Figure 8 shows the envelope curves of moment versus drift ratio (M-θ_d). Eight specimens had nearly identical initial stiffness. The descending branches of the envelope curves had discrepancies.

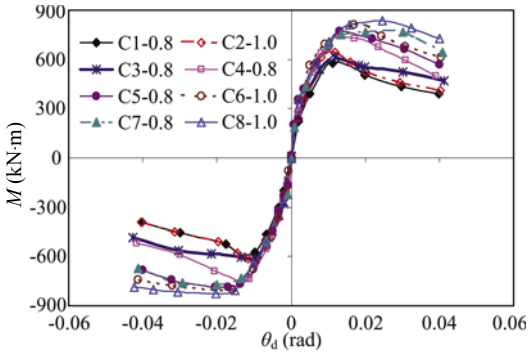

Fig. 8 Moment-drift ratio (M–θ_d) envelope curves of specimens

3.3 Load-carrying capacity

The measured nominal yield moment M_y and the peak moment M_p of the specimens are listed in Table 4, which are the average value measured in the push and pull directions. The nominal yield point was determined by using the method proposed by Park *et al*. (1982). The following findings were obtained.

(1) The nominal yield moment is approximately 0.84 times and 0.74 times the peak moment for specimens C1-0.8 through C4-0.8 and for specimens C5-0.8 through C8-1.0, respectively.

(2) Comparison of three pairs of specimens, i.e., C1-0.8 versus C2-1.0, C5-0.8 versus C6-1.0 and C7-0.8versus C8-1.0, indicates that when the design axial force ratio increases from around 0.8 to 0.95, the peak moment increases by 6.95% on average.

(3) Comparison of C1-0.8 with C4-0.8 indicates that when the area ratio of the the square steel tube increases from 7.68% to 10.2%, the peak moment increases by 27.7%.

(4) Comparison of C1-0.8 with C3-0.8 indicates that when the wall thickness of the circular steel tube increases from 5.62 mm to 9.57 mm, the peak lateral force increases by 5.0%.

(5) A comparison of C1-0.8 with C5-0.8 and C7-0.8, C2-1.0 with C6-1.0 and C8-1.0 indicates that when the width-to-thickness ratio of the square steel tube reduces from 50.1 to 24.5, the peak moment increases by 33.4% and 32.6%, and by 25.2% and 29.0%, respectively.

Table 4 Measured load-carrying capacity of specimens

Specimen No.	M_y (kN·m)	M_p (kN·m)	M_y/M_p
C1-0.8	497.0	583.6	0.85
C2-1.0	549.2	643.2	0.85
C3-0.8	511.3	612.6	0.83
C4-0.8	618.7	745.0	0.83
C5-0.8	581.2	778.5	0.75
C6-1.0	615.8	805.1	0.76
C7-0.8	575.8	773.8	0.74
C8-1.0	599.0	829.6	0.72

3.4 Deformation capacity

Table 5 presents the nominal yield lateral displacement Δ_y, peak lateral displacement Δ_p, ultimate lateral displacement Δ_u, and the corresponding drift ratios for all specimens. The values shown in Table 5 are the average displacement measured in the push and pull directions. The nominal yield displacement and the peak displacement are the displacement corresponding to the nominal yield moment and to the peak moment of the specimens, respectively. The ultimate displacement is defined as the post-peak displacement corresponding to the moment decreases to 85% of the peak value.

The test results indicate that:

(1) The peak drift ratio $\theta_{d,p}$ of the specimens is larger than 1/100 except specimen C2-1.0, which has a peak

Table 5 Deformation capacity of specimens

Specimens No.	Nominal yield		Peak		Ultimate	
	Δ_y (mm)	$\theta_{d,y}$ (rad)	Δ_p (mm)	$\theta_{d,p}$ (rad)	Δ_u (mm)	$\theta_{d,u}$ (rad)
C1-0.8	9.21	1/130	16.47	1/73	25.63	1/47
C2-1.0	7.98	1/150	11.90	1/101	21.21	1/57
C3-0.8	8.14	1/147	12.94	1/93	40.71	1/29
C4-0.8	9.61	1/125	15.84	1/76	31.68	1/38
C5-0.8	9.36	1/134	18.83	1/66	45.54	1/27
C6-1.0	9.79	1/128	20.44	1/61	54.02	1/23
C7-0.8	9.74	1/128	28.35	1/44	51.70	1/24
C8-1.0	9.96	1/126	28.07	1/45	52.87	1/24

drift ratio $\theta_{d,p}$ of 1/101, almost being close to 1/100.

(2) Comparison of specimen C1-0.8 with C3-0.8 indicates that an increasing thickness of the circular steel tube from 5.62 mm to 9.57 mm leads to an increase in the ultimate drift ratio by 58.8%.

(3) Comparison of specimen C1-0.8 with C4-0.8 indicates that increasing the area ratio of the square steel tube from 7.68% to 10.2% leads to an increase in the ultimate drift ratio by 23.6%.

(4) Comparing specimen C1-0.8 to C5-0.8 and C7-0.8, specimen C2-1.0 to C6-1.0 and C8-1.0, reducing the β_1 value from 50.1 to 24.7, the ultimate drift ratio increases 77.7% and 101.7%, 154.7% and 149.3%, respectively.

(5) Comparison of specimen C1-0.8 with C2-1.0 indicates that increasing the axial force ratio leads to a decreased ultimate drift ratio for the specimens with a β_1 value of 50.1. However, for specimens C5-0.8 through C8-1.0, of which the square steel tube has a β_1 value of 24.5, the deformation capacity does not change much when the design value of the axial force ratio varies from 0.78 to 0.93.

(6) Comparison of specimen C5-0.8 with C7-0.8, and specimen C6-1.0 with C8-1.0 indicates that welding the stiffeners to the circular steel tube does not affect the deformation capacity of the specimens.

3.5 Energy dissipation capacity

Figure 9 shows the cumulative energy dissipation curves for all specimens. The energy dissipated in each loading cycle is defined as the area enclosed by the corresponding moment-drift ratio (M-θ_d) hysteretic loop. The cumulative energy dissipation corresponding to drift ratio θ_d is the energy dissipated at drift ratio θ_d sums up that at all of the previous drift ratios. Note that the cumulative energy dissipation capacity for specimens C5-0.8 through C8-1.0 is about 2.75 times that for specimens C1-0.8 through C4-0.8.

Figure 10 shows the equivalent damping ratio - drift ratio (h_e-θ_d) curves of all the specimens. When the drift ratio is smaller than 1/33, the equivalent damping ratio of specimens C1-0.8 through C4-0.8 is less than that of specimens C5-0.8 through C8-1.0. When the drift ratio is 1/25, only specimen C2-1.0 has an equivalent damping ratio larger than specimens C7-0.8 and C8-1.0, and the equivalent damping ratio of specimens C1-0.8, C3-0.8 and C4-0.8 is smaller than for specimens C5-0.8 through C8-1.0.

The test results indicate that the CFDT columns with a β_1 value of 24.5 have larger energy dissipation capacity than CFDT columns with a β_1 value of 50.1.

3.6 Average secant stiffness

The average secant stiffness of the test columns is defined as:

$$K_i = \frac{\sum_{j=1}^{m}(|+P_{i,j}|+|-P_{i,j}|)}{\sum_{j=1}^{m}(|+\Delta_{i,j}|+|-\Delta_{i,j}|)} \tag{3}$$

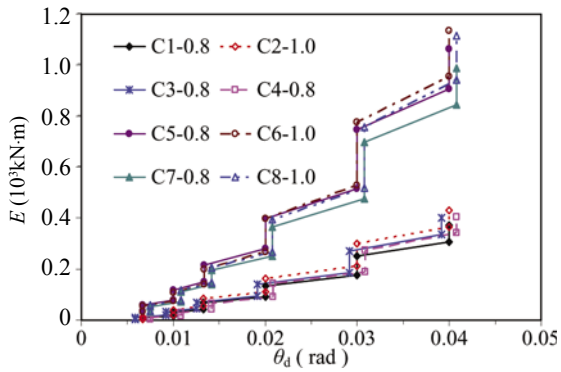

Fig. 9 Cumulative energy dissipation curves for specimens

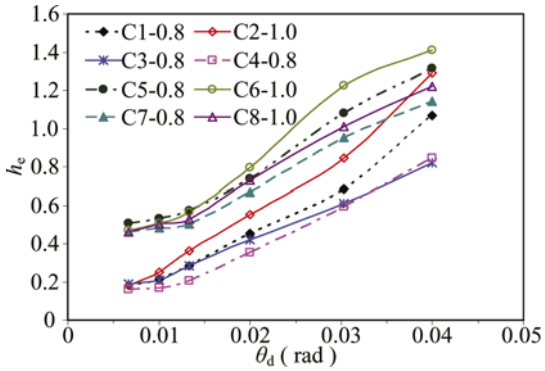

Fig. 10 Equivalent hysteretic damping coefficient curves for specimens

Table 6 Average secant stiffness of specimens

θ_d (rad)	K (10^4 kN/m)							
	C1-0.8	C2-1.0	C3-0.8	C4-0.8	C5-0.8	C6-1.0	C7-0.8	C8-1.0
1/1000	9.53	10.66	11.49	11.47	10.41	11.57	11.03	10.39
1/500	7.21	7.97	8.88	8.75	8.09	9.57	8.23	8.06
1/300	6.01	7.06	7.01	7.24	6.84	7.01	6.55	7.72
1/200	5.08	6.11	5.70	6.20	5.50	6.00	5.38	5.79
1/150	4.47	5.30	4.90	5.46	4.78	4.90	4.70	4.98
1/100	3.51	3.96	3.75	4.41	3.89	3.59	3.92	3.92
1/75	2.59	2.56	2.65	3.53	3.16	2.97	3.19	3.18
1/50	1.43	1.35	1.51	2.09	2.10	2.04	2.11	2.16
1/33	0.72	0.66	0.84	1.03	1.18	1.14	1.24	1.31
1/25	0.36	0.36	0.50	0.54	0.86	0.87	0.90	0.98

where K_i denotes the average secant stiffness at drift ratio $\theta_{d,i}$; $\Delta_{i,j}$ and $P_{i,j}$ denote the maximum displacement and the corresponding lateral load, respectively, under the jth loading cycle at drift ratio $\theta_{d,i}$; and m denotes the number of loading cycles at drift ratio $\theta_{d,i}$. The average secant stiffness of all specimens is listed in Table 6. Figure 11 shows the average secant stiffness degradation curves of all the specimens.

In general, as the axial force ratio and area ratio of the square steel tube or wall thickness of the circular steel tube increases, or as the width-to-thickness of the square steel tube decreases, the initial average secant stiffness at drift ratio of 1/1000 may increase. Specimens with a large width-to-thickness ratio of the square steel tube exhibit more rapid degradation of average secant stiffness.

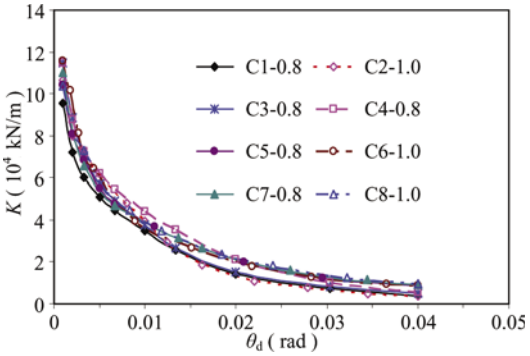

Fig. 11 Average secant stiffness degradation curves of specimens

3.7 Strains

Lateral force versus steel tube strain (P-ε) hysteretic loops of specimen C1-0.8 are shown in Fig. 12, where the positive and negative values of strains correspond to tension and compression, respectively. The strains were measured by the strain gauges, which were mounted at 30 mm height above the column base. In Fig. 12, A, B and C marked in the hysteretic loops are the nominal yield point, peak point and ultimate point in push, respectively, and D is the peak point in pull; ε_y denotes the yield strain of steel tube material as listed in Table 3.

Test results indicate that the lateral strains of the square and circular steel tube were in tension while the test was in progress. At the peak point in push, the lateral strain of the square steel tube reached the yielding, and it was close to the yielding for the circular steel tube. At the peak point in pull, the lateral strains of the square and circular steel tube did not yield. At the nominal yield point in push, the vertical compressive strains of both the square and circular steel tubes were greater than the yield strain; at the peak point in pull, the vertical tensile strains of both the square and circular steel tubes had already yielded.

Figure 13 displays the average vertical strain distribution along the square steel tube section height of specimens C1-0.8 through C4-0.8 at the peak moment. The average vertical strains were obtained from the LVDTs measured vertical deformation of the square steel tube from its bottom up to a height of 300 mm.

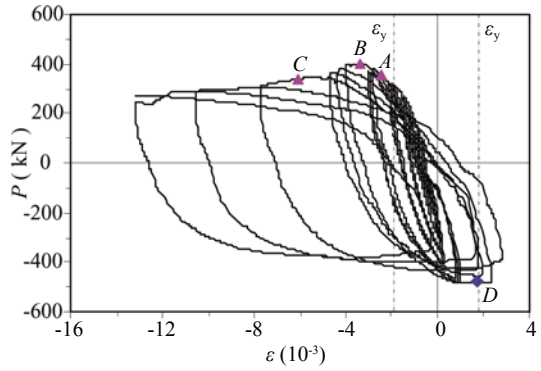

(a) Vertical strain of the circular steel tube

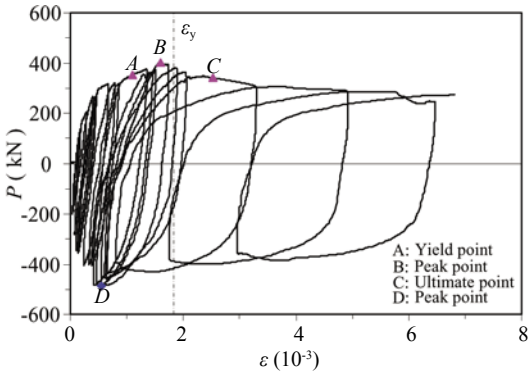

(b) Lateral strain of the circular steel tube

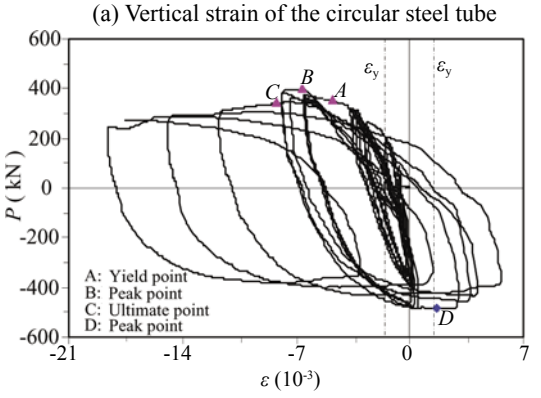

(c) Vertical strain of the square steel tube

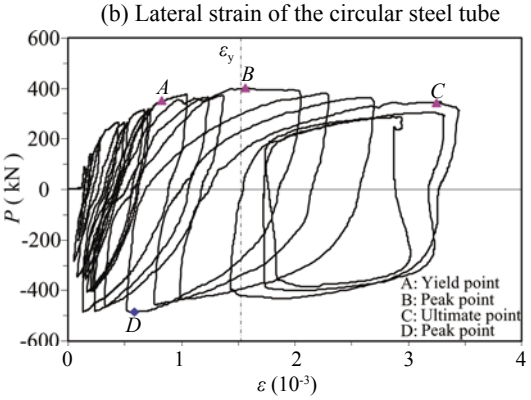

(d) Lateral strain of the square steel tube

Fig. 12 Hysteretic loops of lateral force-steel tube strain (P-ε) of specimen C1-0.8

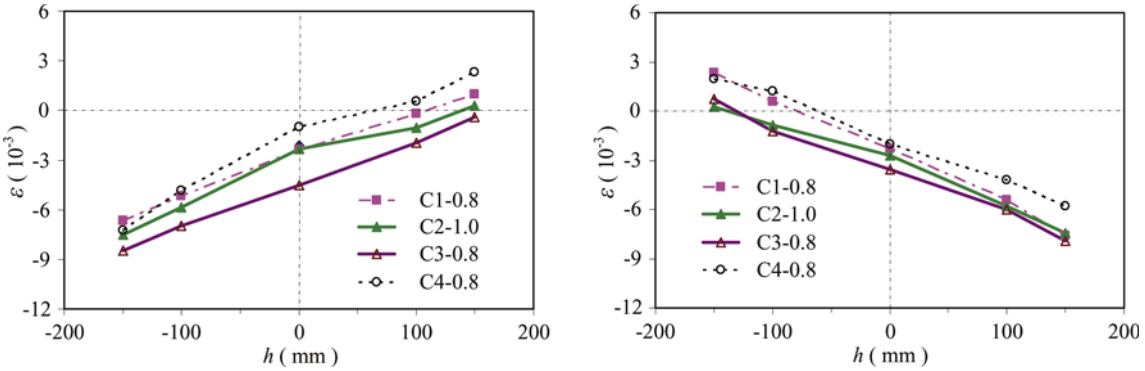

(a) In push (b) In pull

Fig. 13 Average vertical strain distribution along section height at the bottom part of specimens

It is found that the average vertical strain distribution satisfies the plane section assumption.

4 Conclusions

Based on quasi-static test results of eight CFDT column specimens, the following conclusions are reached.

(1) The width-to-thickness ratio of the square steel tube obviously affects the damage development of the CFDT columns. For columns with a ratio of 50.1 and 24.5, local buckling of the square steel tube was found at a drift ratio of 1/150 and 1/50, respectively. After the 1/25 drift ratio loading, the columns with the ratio of 50.1 yielded much more severe residual buckling deformation than the columns with the ratio of 24.5.

(2) The lateral force-displacement hysteretic loops are plump and stable for all specimens. The cumulative energy dissipation capacity and the equivalent hysteretic damping coefficient for the test columns with a width-to-thickness ratio of the square steel tube of 24.5 is larger than the test columns with a ratio of 50.1.

(3) Reducing the width-to-thickness ratio of the square steel tube, increasing the area ratio of the square steel tube, increasing the design value of the axial force ratio from 0.8 to 1.0, or increasing the wall thickness of the circular steel tube, leads to an increased flexural strength of the CFDT columns.

(4) Decreasing the width-to-thickness ratio of the square steel tube, increasing the area ratio of the square steel tube, or increasing the wall thickness of the circular steel tube, leads to an increased ultimate deformation capacity as well as an increased initial average secant stiffness at a drift ratio of 1/1000 for the CFDT columns.

(5) At the lower portion of the test CFDT columns, the measured average vertical strain distribution along the section height satisfies the plane section assumption at the peak moment.

Acknowledgement

The research presented herein was supported by the National Natural Science Foundation of China (Grants Nos. 51261120377 and 51008173). The writers wish to express their sincere gratitude to the sponsors.

References

Cai SH (1999), "Recent Development of Steel Tube-Confined Concrete Structures in China," *China Civil Engineering Journal*, **32**(4): 16–26. (in Chinese)

Cai SH and Jiao ZH (1984), "Behavior and Ultimate Strength of Short Concrete-filled Steel Tubular Columns," *Journal of Building Structures*, **5**(6): 13–29. (in Chinese)

Eiichi Inai1, Akiyoshi Mukai, Makoto Kai *et al*. (2004), "Behavior of Concrete-filled Steel Tube Beam Columns," *Journal of Structural Engineering*, ASCE, **130**(2): 180–188.

Gardner NJ and Jacobson ER (1967), "Structural Behavior of Concrete Filled Steel Tubes," J*ournal of American Concrete Institute*, **64**(7): 402–412.

Knowles RB and Park R (1969), "Strength of Concrete Filled Steel Tubular Columns," *Proceedings of ASCE*, *Journal of the Structural Division*, **12**: 2565–2587.

Liew Richard JY and Xiong DX (2012), "Ultra-high Strength Concrete Filled Composite Columns for Multi-Story Building Construction," *Advances in Structural Engineering*, **15**(9): 1487–1503.

Lü TQ and Zhao GF (2001), "Numerical Method for Analysis of Ultimate Strength of Concrete-filled Square Steel Tubular Columns under Eccentric Compression Reinforced by Inner Circular Steel Tube," *Journal of Dalian University of Technology*, **41**(5): 612–616. (in Chinese)

Ministry Standard of the People's Republic of China (2010), *Technical Specification for Concrete Structures of Tall Building* (*JGJ3-2010*), Ministry of Construction

of Peoples Republic of China, Beijing: China. (in Chinese)

National Standard of the People's Republic of China (2010), *Code for Design of Concrete Structures* (*GB 50010-2010*), Ministry of Construction of Peoples Republic of China, Beijing: China. (in Chinese)

Park R, Priestley MJN and Gill WD (1982), "Ductility of the Square-confined Concrete Columns," *Journal of the Structural Division*, ASCE, **108**(4): 929–950.

Pei WJ (2005), *Research on Mechanical Performance of Multi-Barrel Tube-Confined Concrete Columns*. Chang'an University. (in Chinese)

Qian JR, Zhang Y, Ji XD and Cao WL (2012), "Test and Analysis of Axial Compressive Behavior of Composite-Sectioned High Strength Concrete Filled Steel Tube Short Columns," *Journal of Building Structures*, **32**(11): 68–76. (in Chinese)

Randall VR and Foot KB (1989), "High Strength Concrete for Pacific First Center," *Concrete International Design and Construction*, **11**(4):14–16.

Rangan BV and Joyce M (1992), "Strength of Eccentrically Loaded Slender Steel Tubular Columns Filled High-strength Concrete," *ACI Structural Journal*, **9**(6): 676–681.

Roik K and Bergmann R (1985), "Composite Column Design and Examples for Construction," *Composite and Mixed Construction*, *Procs. of the US/Japan Joint Seminar*, Seattle, July 18-20, 1984, ASCE, New York: 267–278.

Sugiki H, Suziki S and Ooguru T (1998), "Design and Construction of a 55-story Apartment Building Used CFT Columns," *Concrete Engineering*, **1998**(2): 27–31. (in Japanese)

Varma AH, Ricles JM, Sause R and Lu LW (2004), "Seismic Behavior and Design of High-strength Square Concrete-filled Steel Tube Beam Columns," *Journal of Structural Engineering*, ASCE, **130**(2): 169–179.

Webb J and Peyton JJ (1990), "Composite Concrete Filled Steel Tube Columns," *Procs. of 2nd National Structural Conference of Australia*. The Institution of Engineers, Australia, Adelaide: 181–185.

Wu GL and Hua Y (2002), "Application of Concrete Filled Steel Tubular Column in Super High-rise Building-SEG Plaza," *Proceedings of ASCCS Conference*, Edited by Xiao Y and Mahin SA, Los Angeles, USA, **1**:77–83.

Ye LP (2012), *Design of Concrete Structures*. Beijing: China Architecture & Building Press. (in Chinese)

Zhang YF, Zhao JH and Li XW (2009), "On the Axial Bearing Capacity of Composite Concrete-filled Steel Tubes Based on the Unified Theory," *Journal of Xi'an University of Architecture & Technology* (*Natural Science Edition*), **41**(1): 41–46. (in Chinese)

Zhang ZG and Zuo MS (1985), "Behavior of Concrete Filled Square Steel Tube Short Columns under Centrally Loading," *Journal of Zhengzhou University of Technology*, **2**: 19–32. (in Chinese)

Zhong ST and Wang YC (1980), "Research on Analysis Theory of Axial Compression Member of Concrete Filled Steel Tubes," *Journal of Building Structures*, **1**(1): 61–71. (in Chinese)